for this composition. In the case of 90.1 mol% AgI, metal-plate press quenching produces only β-AgI (Fig. 1c), as in the case of 87.6 mol% AgI. When twin-roller quenching is used, however, the diffraction peaks due to α-AgI are clearly observed (Fig. 1d), and the peak intensity increases with increasing cooling rate, as shown in Fig. 1e. It is thus obvious that both the composition and the melt-cooling rate are very important for obtaining α-AgI at ambient temperature.

Figure 2 is a phase diagram to show which phases are obtained when the cooling rate and the chemical composition are changed. Different symbols represent different phases obtained during melt quenching. Open squares denote the glassy phase. Double circles mean that only the α-AgI phase was observed. Open circles and open triangles indicate the co-existence of α- and β-phases; the α-phase is dominant in open circles and the β-phase in open triangles. Closed circles denote that only the β-AgI phase was observed. It is seen that the α-AgI phase is frozen only when the AgI content is slightly larger than that in the glass-forming limit. The cooling rate should also be higher than 10^5 K s^{-1} to obtain α-AgI at ambient temperature. Although the $\alpha \rightarrow \beta$ transformation in AgI crystal morphology occurs extremely rapidly[19], we suggest that the increase in the viscosity of the matrix melts (undercooled liquids) during cooling prevents the $\alpha \rightarrow \beta$ transformation of the precipitated α-AgI to the β-phase; the cooling rate, and thus the rate of increasing viscosity, is very large in the case of twin-roller quenching.

Figure 3 shows the temperature dependence of conductivity for a twin-roller-quenched sample of 90.1 AgI·9.9 Ag$_3$BO$_3$ in which α-AgI is frozen in the matrices. The conductivity of an AgI crystal flake prepared by twin-roller quenching of pure AgI crystal is also shown for comparison. The conductivity at ambient temperature for samples with frozen-in α-AgI is $\sim 10^{-1}$ S cm^{-1}; such an extremely high ion conductivity is expected if composites composed of frozen α-AgI and superionic conducting glasses are formed. The activation energy in the temperature range 25 to 140 °C was 15 kJ mol^{-1}. These values are reasonable if the frozen α-AgI phase is present as highly dispersed, discrete particles, the conductivity of which was

calculated by Maxwell's equation for the conductivity of composite materials[20]. With increasing temperature, a small conductivity change is observed near the $\alpha \rightarrow \beta$ transformation temperature of 147 °C, which is probably due to small amounts of residual β-phase. With decreasing temperature, however, no change in conductivity is observed at 147 °C, and the conductivity starts to decrease considerably at ~ 110 °C. The conductivity decrease is due to the $\alpha \rightarrow \beta$ transformation of the AgI crystal in the glass matrices; the cooling runs of high-temperature X-ray diffraction measurements for this sample confirm that this transformation occurs. This result indicates that even if the cooling rate is small, as in the conductivity measurements, glass matrices with high viscosity depress the $\alpha \rightarrow \beta$ transformation. Preliminary experiments for glass matrices other than borates indicate that a viscosity effect is likely; the details will be reported elsewhere. □

1. Tubandt, C. & Lorenz, E. Z. phys. Chem. 24, 513–543 (1914).
2. van Gool, W. (ed.) Fast Ion Transport in Solids (North-Holland, Amsterdam, 1973).
3. Funke, K., Prog. Solid State Chem. 11, 345–402 (1976).
4. Bradley, J. N. & Greene, P. D. Trans. Faraday Soc. 63, 424–430 (1967).
5. Suchow, L. & Pond, G. R. J. Am. chem. Soc. 75, 5242–5244 (1953).
6. Takahashi, T., Ikeda, S. & Yamamoto, O. J. electrochem. Soc. 120, 647–651 (1973).
7. Takahashi, T., Ikeda, S. & Yamamoto, O. J. electrochem. Soc. 119, 477–482 (1972).
8. Minami, T., Nambu Y. & Tanaka, M. J. Am. Ceram. Soc. 60, 467–469 (1977).
9. Minami, T., Imazawa, Y. & Tanaka, M. J. non-cryst. Solids 42, 469–476 (1980).
10. Minami, T. J. non-cryst. Solids 95/96, 107–118 (1980).
11. Minami, T., Takuma, Y. & Tanaka, M., J. electrochem. Soc., 124, 1659–1662 (1977).
12. Wnetrzewski, B., Nowinski, J. L. & Jakubowski, W. Solid State Ionics 36, 209–211 (1989).
13. Minami, T., Ikeda, Y. & Tanaka, M. Nippon Kagaku Kaishi, 1617–1623 (1981).
14. Tatsumisago, M. & Minami, T. Mater. Chem. Phys. 18, 1–17 (1987).
15. Sarjeant, P. T. & Roy, R. J. Am. Ceram. Soc. 50, 500–503 (1967).
16. Sarjeant, P. T. & Roy, R. Mater. Res. Bull. 3, 265–280 (1968).
17. Nakamura, T. & Takashige, M. Kotaibutsuri 15, 497–503 (1980).
18. Tatsumisago, M., Machida, N. & Minami, T. J. Ceram. Soc. Japan 95, 59–63 (1987).
19. Burley, G. Acta Cryst. 23, 1–5 (1967).
20. Kingery, W. D., Bowen, H. K. & Uhlmann, D. R. Introduction to Ceramics 634–643 (Wiley, New York, 1975).
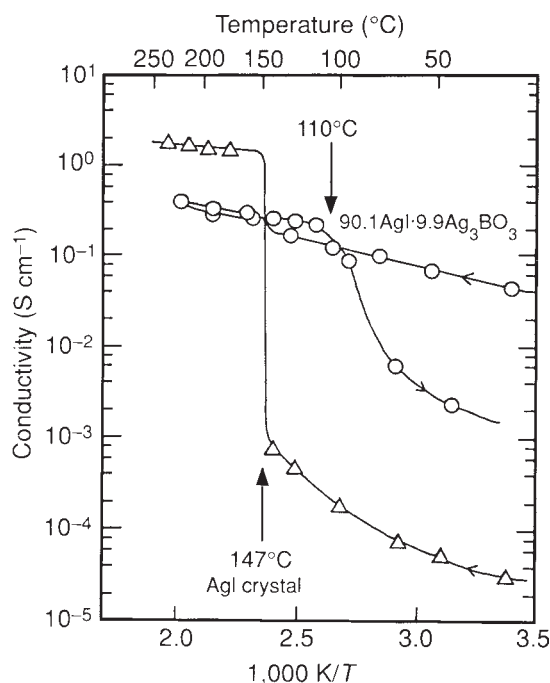
FIG. 3 Temperature dependence of conductivity for the twin-roller quenched samples of 90.1 AgI·9.9 Ag$_3$BO$_3$, in which α-AgI is the main component of the crystals, and for a crystal of AgI.

Effect of defects on molecular mobility in liquid water

Francesco Sciortino*, Alfons Geiger†
& H. Eugene Stanley*

* Center for Polymer Studies and Department of Physics, Boston University, Boston, Massachusetts 02215, USA
† Physikalische Chemie, Fachbereich Chemie der Universität Dortmund, Postfach 500500, D-4600 Dortmund 50, Germany

LIQUID water is a totally connected random network of hydrogen bonds, the connectivity lying well above the percolation threshold[1-3]. But despite this extensive association of hydrogen bonds with strengths greater than the thermal energy, the diffusion and rotation rates of water molecules at ambient temperatures are comparable to those of non-associated simple liquids. Many experiments have indicated that the random tetrahedral network cannot be perfect but must contain defects, which are characterized geometrically by the presence of an extra (fifth) molecule in the first coordination shell, or topologically by the presence of 'bifurcated' hydrogen bonds[4-7]. Here we use molecular-dynamics simulations to examine the effect of such defects on molecular mobility in water. We find that they provide pathways of lower energy between different tetrahedral local arrangements, thus acting as 'catalysts'. The anomalous mobility of water under compression[8,9] and the decreased mobility in hydrophobic hydration shells[10,11] can be interpreted on the same basis. We suggest that our results are relevant to studies on 'stretched' water[12,13].

We have used two parallel approaches. The first is to change the global concentration of defects in the system: we tune the defect concentration not by changing the temperature but by changing the density of the simulated system[14]. This method enables us to distinguish between contributions to the mobility arising from thermal effects and those related to the defect concentration. The second approach is to compare the properties of groups of molecules that all belong to the same system but have different numbers of nearest neighbours. Using these two approaches, we can relate global behaviour to a microscopic picture based on the 'catalytic activity' of extra molecules.

In both approaches, we analyse quenched configurations, which represent the inherent structure of the liquid[15]. Because only local minima survive the quench process, the quenched
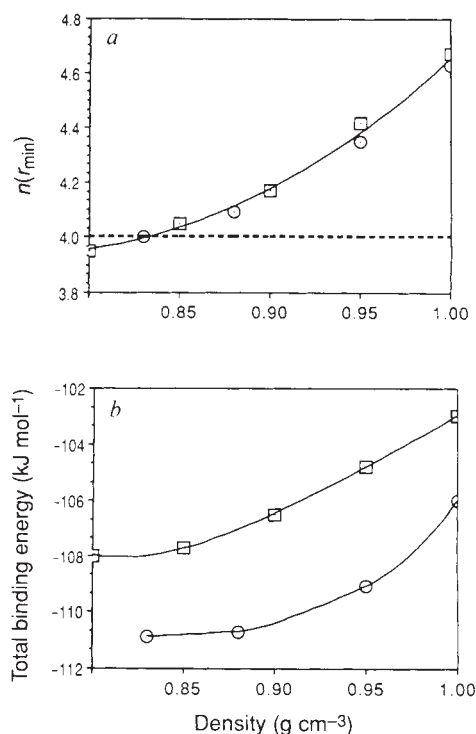
state represents the structure of the liquid without vibrational distortions. By analysing the bonding and structure after these thermal vibrations have been subtracted, we are able to make a clear distinction between purely thermal displacements and 'inherent' defects[16], and to separate the effects on molecular mobility owing to network topology from those resulting simply from thermal excitation.

We study changes in local structure as a function of the global density of the system by looking at the changes in the first coordination shell. In Fig. 1a we show the average number of molecules $\langle n(r_{min}) \rangle$ within a sphere of radius $r_{min} = 3.3$ Å as a function of the average density. Here r_{min} is the position of the first minimum in the radial distribution function. At density $\rho = 1$ g cm^{-3}, there are ~4.6 neighbours; as ρ is lowered there is a progressive decrease until a value of 4.0 is reached at $\rho \approx 0.85$.

The average binding energy of the water molecules also decreases (Fig. 1b) as ρ is decreased. Thus Fig. 1a indicates that progressive 'stretching' of water leads to more tetrahedral bonding, and Fig. 1b demonstrates that stretching strengthens bonding.

Even at microscopic scales, a higher (less negative) binding energy is associated predominantly with a higher local density. To see this, we first calculate $P(E_i)$, the histogram of number of molecules with total binding energy E_i (Fig. 2a). For each energy bin, we then calculate the average coordination number $\langle n(r_{min}) \rangle_{E_i}$ (Fig. 2b). We find that the average coordination number is enhanced for energies above the 'tetrahedral network' peak in $P(E_i)$, at ~ -115 kJ mol^{-1}, demonstrating that high-energy states (above -115 kJ mol^{-1}) are associated with a denser local environment.

FIG. 1 Density dependence in ST2 water at 273 K ($\square$) and 235 K ($\bigcirc$) for a, the average number of neighbours inside a shell of radius $r_{min} = 3.3$ Å, and b, the average total binding energy $E_i = \sum_j V_{ij}$; here V_{ij} is the pair interaction energy between molecules i and j. Both quantities are calculated using quenched configurations. Our simulations concern a system of 216 water molecules interacting via the ST2 potential[23] (we found similar results for SPC[24] and TIP4P[25] potentials). Thus we perform simulations at a constant density and constant energy (the NVE ensemble). The direct molecular interactions up to the cutoff distance $r_c = 7.8$ Å are combined with a reaction field approximation for more distant pairs. The density is decreased in steps from $\rho = 1.0$ g cm^{-3} to 0.8 g cm^{-3}. Two parallel simulation series were performed, with average temperatures of 273 and 235 K. Before the actual simulations were started, equilibration runs (extending up to 300 ps at low temperatures or densities) were applied. For a further description of the computational techniques, see ref. 21. We choose to study the 'low' temperature of $T = 235$ K to facilitate the recognition of effects related to the temperature. From each simulation we extract 50–100 equally spaced configurations (corresponding to a time interval between configurations ranging from 0.2 to 0.6 ps). We then calculate the respective 'quenched' (or 'inherent') configurations using a two-stage procedure[15]: (1) the equations of motion are strongly damped to remove the kinetic energy quickly; (2) the molecules are moved along the potential-energy surface toward the local minimum by means of a steepest-descent numerical calculation. This steepest-descent procedure is performed until the change in potential energy between successive steps is less than 10^{-5} kJ mol^{-1} (we tested our results by performing a calculation using 10^{-6} kJ mol^{-1}, and we found essentially the same results).
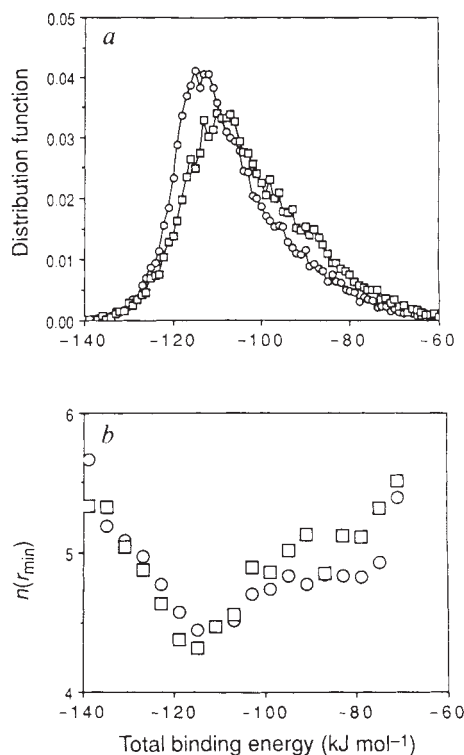

FIG. 2 a, Distribution function $P(E_i)$ for the binding energy $E_i = \sum_j V_j$ calculated using the quenched configurations. Symbols: $T = 273$ K ($\square$) and 235 K ($\bigcirc$). The average density here is $\rho = 1.0$ g cm^{-3}. b, $\langle n(r_{min}) \rangle_{E_i}$, the number of neighbours inside a shell of radius 3.3 Å, averaged over all the molecules with the same E_i, as a function of the binding energy E_i. Note the enhancement for energies below, as well as above, the central 'perfect tetrahedral network' peak in $P(E_i)$ at ~ -115 kJ mol^{-1}. The total potential energy of the system is, with our definition, $\frac{1}{2}\sum_i E_i$, as each interaction V_{ij} is counted twice.
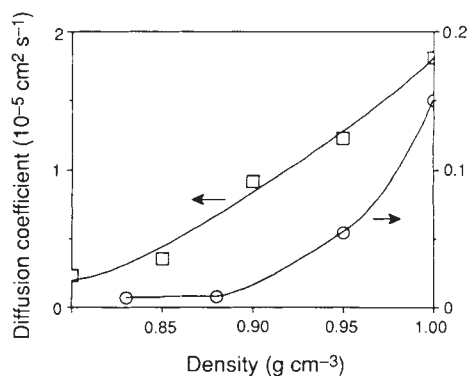
FIG. 3 Density dependence in ST2 water at 273 K (□) and 235 K (○) for the diffusion coefficient. The diffusion coefficients are calculated from the long-time limit of the slope of a graph of mean square displacement against time.

An additional important observation from Fig. 2 is that there are a few very sparsely populated low-energy states (below $-115 \, kJ \, mol^{-1}$) that possess a high local density. An extra molecule can therefore fit in the first coordination shell in such a way as to decrease (that is, strengthen) the total bonding energy. This can be understood if there exists a 'bonded state' with more than four strong interactions: in other words, if some hydrogen bonds are bifurcated. There are two different local geometries for the molecules that produce such a low energy state. In one configuration, the central water molecule shares one of its protons between two neighbour oxygens; in the other configuration, one of the two lone pairs accepts protons from two different molecules. In both cases, the central molecule has five neighbours instead of four. That such bifurcated bonds can occur is well known from hydrate crystals[17]. Our interpretation is supported by quantum mechanical calculations on water molecule clusters, which demonstrate that a symmetric[18] or asymmetric[19] energy-optimized bifurcated hydrogen bond is stronger than a conventional linear bond ($\delta E \approx -4 \, kJ \, mol^{-1}$), and by experimental results[20] that can be interpreted in terms of the existence of four- and five-bonded water molecules[21].

If the mobility of the liquid were related to the local density as expected from a picture of local free volume[22], then one would expect the molecular mobility to increase as the density decreases. Instead, the opposite trend is observed[14]; Fig. 3 shows the density dependence of the self-diffusion coefficient, D, which we calculate from the mean square displacement. We find that lowering the density by 10% (from 1.0 to 0.9) decreases the diffusivity by a factor of two at 273 K, and by a factor of 10 at 235 K. We find a similar sensitivity to density for the times taken for the molecules to re-orient.

These results can be used to provide a microscopic support for the hypothesis that switching from one 'regular' hydrogen bond arrangement to another is facilitated by the local arrangement associated with higher local density. Accordingly, we relate structural data extracted from the quenched configurations to dynamical data extracted from the corresponding original molecular dynamics sequences. We calculate the mean square displacement $\langle r^2(t) \rangle_n$ for groups of molecules with numbers of neighbours $n = 4$, 5 and 6 (Fig. 4a). We observe a significantly higher mobility for molecules with more than four neighbours, confirming that molecular mobility is enhanced in the presence of 'extra' molecules in the first coordination shell.

To confirm that the higher mobility of the five-coordinated molecules compared with four-coordinated molecules is not simply a result of different bonding energies, we plot in Fig. 4b the mean square displacement for five- and four-coordinated molecules with the same E_i. We see that the five-coordinated molecules have a higher mobility than the four-coordinated molecules. Analogous results are obtained for rotational diffusion.

Our results support the possibility that the presence of an 'extra' molecule (in the first coordination shell) lowers the energy barriers for translational as well as rotational motions, and that the faster dynamics are not due to a weaker local bonding, but to a progressive reduction of the tetrahedral symmetry of the local minima in the potential-energy surface and the introduction of new local minima. Thus the extra molecule can 'catalyse' the restructuring of the hydrogen bond network when the thermal energy kT is much smaller than the hydrogen bond energy. An analogy with the influence of inert (hydrophobic) solutes is
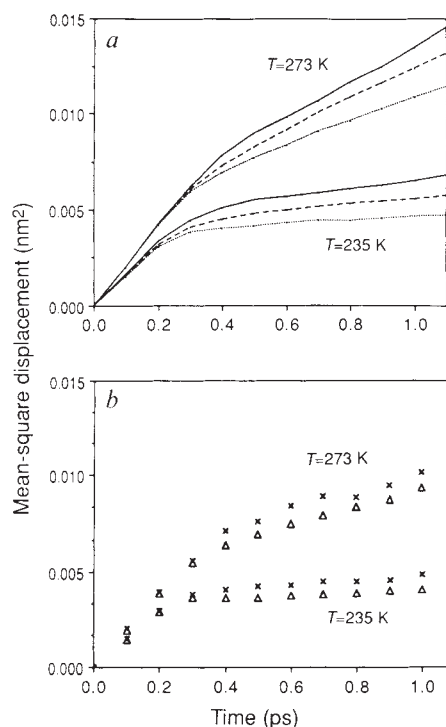
FIG. 4 a, Mean square displacement $\langle r^2(t) \rangle_n$ for groups of molecules with number of neighbours n equal to four (———), five (– – – –) and six (· · · ·) for $T = 235$ and 273 K. b, Mean square displacement $\langle r^2(t) \rangle_{n,E_i}$ for molecules with four (△) and five (×) neighbours and binding energy E_i between -110 and $-115 \, kJ \, mol^{-1}$. The E_i bin between -110 and $-115 \, kJ \, mol^{-1}$ has been selected because in this range one can find a sufficiently large number of both 5- and 4-coordinated molecules. As seen in Fig. 2, the average coordination number for this range of energies is ~4.5. $\langle r^2(t) \rangle_n$ is calculated by following the time development of molecules for a time interval of 1.2 ps centred on a selected quenched configuration. The classification of the molecules according to the number of neighbours n is performed on the quenched configuration at the time $t = 0.6$ ps. The average density here is $1.0 \, g \, cm^{-3}$.

helpful. The decreased mobility and the increased structural order in hydrophobic hydration shells[10,11] can be understood as consequences of the lower local density of water, which arise because the water is effectively locally diluted by the hydrophobic particle. The presence of the inert hydrophobic particle prevents the water molecules in the hydration shell being approached by more than four other molecules; this prevents the creation of low-activation-energy barriers and slows down the molecular mobility (this idea has received recent experimental support: see U. Kaatze and R. Pottel, preprint). The opposite effect—the creation of increased mobility by increasing the (global) density—is the well known 'anomalous motional behaviour' of water under compression[8,9]. □

1. Angell, C. A. Ann. Rev. Phys. Chem. 34, 593–611 (1983).
2. Dore, J. & Teixeira, J. (eds) Hydrogen Bonded Liquids (Kluwer, Dordrecht, 1991).
3. Stillinger, F. H. Science 209, 451–457 (1980).
4. Grünwald, E. J. Am. chem. Soc. 108, 5719–5726 (1986).
5. Narten, A. H. & Levy, H. A. Science 165, 447–454 (1969).
6. Giguère, P. A. J. chem. Phys. 87, 4835–4839 (1987).
7. Walrafen, G. E., Hokmabadi, M. S., Yang, W.-H., Chu, Y. C. & Monosmith, B. J. phys. Chem. 93, 2909–2917 (1989).
8. Lang, E. W. & Lüdemann, H. D. in High Pressure NMR (ed. Jonas, J.) (Springer, Berlin, 1991).
9. Pottel, R., Asselborn, E., Eck, R. & Tresp, V. Ber. Buns. phys. Chem. 93, 676–688 (1989).
10. Geiger, A., Rahman, A. & Stillinger, F. H. J. chem. Phys. 70, 273–276 (1979).
11. Huot, J.-Y. & Jolicoeur, C. in The Chemical Physics of Solvation (eds Dogonadze, R. R., Kalman, E., Kornyshew, A. A. & Ulstrup, J.) (Elsevier, Amsterdam, 1985).
12. Angell, C. A. Nature 331, 206–211 (1988).
13. Green, J. L., Durben, D. J., Wolf, G. H. & Angell, C. A. Science 249, 649–652 (1990).
14. Geiger, A., Mausbach, P. & Schnitker, J. in Water and Aqueous Solutions (eds Neilson, G. W. & Enderby, J. E.) (Hilger, Bristol, 1986).
15. Stillinger, F. H. & Weber, T. A. J. phys. Chem. 87, 2833–2840 (1983).
16. Weber, T. A. & Stillinger, F. H. J. chem. Phys. 87, 3252–3253 (1987).
17. Falk, M. & Knop, O. in Water: A Comprehensive Treatise (ed. Franks, F.) (Plenum, New York, 1972).
18. Newton, M. D. J. phys. Chem. 87, 4288–4292 (1983).
19. Newton, M. D., Jeffrey, G. A. & Takagi, S. J. Am. chem. Soc. 101, 1997–2010 (1979).
20. Bosio, L., Chen, S. H. & Teixeira, J. Phys. Rev. A27, 1468 (1983).
21. Sciortino, F., Geiger, A. & Stanley, H. E. Phys. Rev. Lett. 65, 3452–3455 (1990).
22. Cohen, M. H. & Turnbull, D. J. chem. Phys. 31, 1164 (1959).
23. Stillinger, F. H. & Rahman, A. J. chem. Phys. 60, 1545–1557 (1974).
24. Berendsen, H. J. C., Postma, J. P. M., von Gunsteren, W. F. & Hermans, J. in Intermolecular Forces (ed. Pullman, B.) 331 (Reidel, Dordrecht, 1981).
25. Jorgensen, W. L., Chandrasekhar, J., Madura, J. D., Impey, R. W. & Klein, M. L. J. chem. Phys. 79, 926 (1983).

Ocean circulation beneath the Ronne ice shelf

K. W. Nicholls, K. Makinson & A. V. Robinson

British Antarctic Survey, Natural Environment Research Council, High Cross, Madingley Road, Cambridge CB3 0ET, UK

THE intimate thermal contact between the base of Antarctic ice shelves and the underlying ocean enables changes in climate to have a rapid impact on the outflow of ice from the interior of Antarctica[1,2]. Furthermore, water modified by passage under ice shelves, particularly in the Weddell Sea, is believed to be an important constituent of Antarctic Bottom Water[3]—a water mass that can be observed as far north as 50° N in the deep oceans[4]. Antarctic Bottom Water is both cold and oxygen-rich, and plays an important part in the cooling and ventilation of the world's oceans. Because of the difficulty in gaining access, the oceanographic regime beneath ice shelves is very poorly sampled[5]. By successfully drilling through the ice, however, we were able to obtain oceanographic data from beneath the largest Antarctic ice shelf, the Ronne–Filchner ice shelf in the southern Weddell Sea. We find that our data agree well with the predictions of a relatively simple oceanographic plume model of sub-ice-shelf circulation[6].

This model can therefore be used with some confidence to investigate the links between climate changes, ice-shelf melting and bottom-water production.

In January 1991, we used a pressurized hot-water drill to penetrate ice 562 m thick, 300 km from the northern limit of the Ronne ice shelf (Fig. 1). The drill was powered by three heat exchangers, providing a total heating power of 240 kW. A borehole pump, installed in an auxiliary borehole, retrieved enough meltwater to remove the need for continuous snow-melting during drilling. In total, 4.5 tonnes of aviation turbine fuel were burned in the heat exchangers, enabling a hole 20–25 cm in diameter to be drilled over a period of about a week, and then to be kept open for a further five days.

A borehole-deployable conductivity–temperature–depth (CTD) and water-sampling system was used to obtain several CTD profiles, and to retrieve five water samples from the ocean beneath the ice shelf (the samples are currently being analysed for isotope content). The accuracy of the temperature sensor on the CTD was 0.01 °C; the accuracy of the derived salinity was 0.015. Sensor calibrations were checked before and after the field work. The graphs in Fig. 2 show the potential temperature and salinity profiles that were obtained over a 17-h period. The upper 120 m of the water column is well mixed, with a potential temperature and salinity of ~ -2.30 °C and 34.53; the potential temperature and salinity over the next 130 m increase first slowly, then relatively rapidly to −2.07 °C and 34.64; from there to the bottom, at 850 dbar (85 bar), there is a slow increase in potential temperature and salinity to maxima of −2.02 °C and 34.65. To place the new data in context, the measured water characteristics have been plotted on a potential-temperature/salinity diagram (Fig. 3), together with the typical characteristics of the principal water masses of the Weddell Sea.

The data are consistent with the theory that the large-scale circulation under ice shelves is dominated by deep thermohaline convection. This theory has been advanced by Robin[7], and expanded by several authors[3,8,9], most recently by Jenkins[6]. Western shelf water (WSW) is formed in the open lead north of the Ronne ice front by salt rejection from sea-ice production[10,] and has a temperature of ~1.9 °C. The theory proposes that it then drains down the sea-floor slope under the ice shelf (Fig. 4) and arrives unmodified at the base of the thick ice flowing off the continent. There the ice depth can be in excess of 1.5 km,
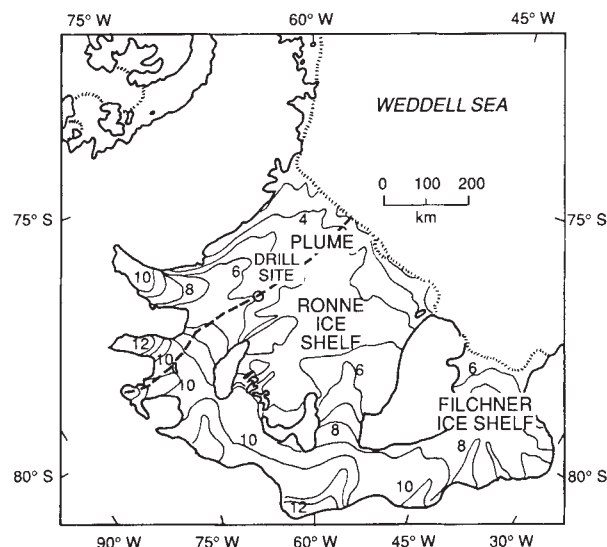

FIG. 1 Map of the Ronne ice shelf showing the location of the drill site (77° 36′ S, 65° 28′ W) and the path of the modelled plume. Contours give ice thickness in hundreds of metres[14].